Energy Efficiency and Communication Accuracy Tradeoff in Intra-body Networks

Pramita Pandit
Temple University
Philadelphia, USA
pramita.pandit@temple.edu

Hirsa Kia
Temple University
Philadelphia, USA
hirsa.kia@temple.edu

Krishna Kant
Temple University
Philadelphia, USA
kkant@temple.edu

Abstract

In this paper, we propose a control scheme that provides a tradeoff between energy efficiency and communication accuracy in the context of intrabody networks designed to manage chronic diseases. We specifically do this in the context of magnetic resonance communications (MRC) technology for communication that we have shown works extremely well for such networks. The key motivation for such a tradeoff is that intrabody networks operate in a very energy-poor environment and thus their energy efficiency is crucial. Our proposed controller uses Kalman filter-based signal reconstruction and adjusts communication frequency based on the signal prediction error. We show that the closed-loop control can reduce the communication by 30-67% with accuracies of 88% to 94%.

ACM Reference Format:
Pramita Pandit, Hirsa Kia, and Krishna Kant. 2025. Energy Efficiency and Communication Accuracy Tradeoff in Intra-body Networks. In *ACM/IEEE International Conference on Connected Health: Applications, Systems and Engineering Technologies (CHASE '25), June 24–26, 2025, New York, NY, USA.* ACM, New York, NY, USA, 6 pages. https://doi.org/10.1145/3721201.3721411

1 Introduction

Chronic diseases are becoming increasingly prevalent worldwide, driven by several factors, including an aging population in developed nations and escalating levels of pollution—air, water, and food—in developing countries [8].

As the risk of multiple chronic conditions rises markedly with advancing age, and with the elderly population expected to nearly double by 2050 [8], there is a pressing need for innovative, cost-effective, and personalized approaches to the prevention and management of chronic diseases.

Recent Advancements in medical devices enable continuous monitoring and automated diagnosis for chronic disease management. A Chronic Disease Management Network (CDMN) is a *small* network of in-body sensors and actuators to improve the functioning of key diseased organs. Examples include managing overactive bladder [9] and pacemakers [4]. A major challenge in CDMNs is ensuring a reliable energy supply, as implanted batteries are impractical due to size constraints and invasive replacement procedures. While energy harvesting from organs or movement is possible, it may be insufficient, necessitating external energy transfer via an On-Body Node (OBN) such as a smartwatch, wristband, or abdominal patch. Wireless Power Transfer (WPT) is essential, alongside extreme energy efficiency in computing and communication. We have explored WPT strategies in [7]. This paper focuses on optimizing intrabody communication as wireless transmission is significantly more energy-intensive than computation. The key contributions of this paper are as follows.

(1) We explore the tradeoff between communication energy consumption vs. accuracy in reporting the signal from sensors. We do this by using a closed-loop control scheme of the signal prediction for sensed samples.
(2) We further explore the tradeoff between accuracy and delay by extending the closed-loop control scheme to batched data transmission from a sensor and batch prediction.

We show that our proposed controller can reduce the communication by 30-67% with accuracies of 88% to 94%. Due to limited space, this paper only considers a typical link in CDMN rather than the network as a whole. We plan to consider the network perspective in future works.

2 Chronic Disease Management Networks

2.1 Communications Architecture of CDMN

The CDMN is structured to efficiently collect physiological signals, with sensors clustered near critical or affected body parts. As shown in Fig. 1, it comprises hub nodes interacting with local sensors/actuators, while only hubs communicate with the OBN. The OBN serves as the central controller, providing energy and interfacing with external networks (e.g., WiFi, BLE).

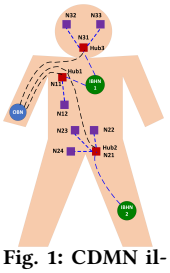

Fig. 1: CDMN illustration

Hubs aggregate sensor data, perform processing, and relay information to the OBN. Sensor nodes receive energy, collect data, and transmit it to hubs. Data flows "upward" from sensors to hubs and the OBN, while control signals propagate "downward." Hub-to-OBN communication is less frequent but energy-intensive.

Since the OBN, akin to a smartwatch, may be removed for charging, a backup wearable (e.g., a stomach patch) ensures continuous alert reception and emergency energy supply. During OBN-off periods, energy-efficient communication becomes critical, aligning with the energy-accuracy tradeoff discussed.

This research was supported by NSF grant CNS-2245088.

CHASE '25, New York, NY, USA

ACM ISBN 979-8-4007-1539-6/2025/06
https://doi.org/10.1145/3721201.3721411

2.2 Communications and Energy Transfer Through the Body

The OBN and backup device utilize specialized antennas for Through-Body Wireless Communication (TBWC) and energy transfer, with all CDMN nodes employing TBWC. This necessitates a low-power Human Body Communication (HBC) technology with a compact antenna and efficient in-body transmission.

It is well known RF is not suitable for HBC [12], but many other technologies have been studied in the literature [11]. Here we focus on Magnetic Resonance Communication (MRC) as our prior work in [3] shows that it is very well suited for CDMN. We have also shown that its performance is competitive with that of Ultrasonic Coupling (USC) [2], a popular HBC technology for medical applications.

Magnetic Resonant Coupling (MRC) employs a resonant transmitter-receiver pair, each forming an LC circuit with a resonance frequency of $1/(2\pi\sqrt{LC})$. While traditionally set at 13.56 MHz (RFID), our extensive experimentation demonstrates that the optimal intrabody performance occurs at 25–30 MHz [6]. We have also shown that the transmission is robust to changes in the relative orientation of transmit and receive coils, and posture/movement of the person, with only 2-3 dB difference across a wide range of parameters [3]. We also show an attenuation level of 15–23 dB over body-length distances, which confirms its feasibility for intrabody networks.

Given the short node distances in CDMN, interference is inevitable, making a fully scheduled MAC layer the most effective solution. With slow sensing rates (one sample per tens of seconds) and tiny packets, scheduling imposes no limitations. The millisecond transmission time allows for low-power modes, conserving energy and facilitating emergency signals without significant delay, though these aspects are beyond this paper's scope.

2.3 Reducing Communication Energy Expense

Communication reduction strategies include lower transmission rates, threshold-based triggering, and sample averaging, though open-loop methods lack adaptability. Instead, a receiver-side predictor adjusts transmission based on reconstruction error.

Among the prediction models, statistical methods are preferred for hubs. ARIMA relies on prior data but assumes stationarity and struggles with missing samples. The Kalman filter, however, models hidden states, enabling robust predictions without stationarity constraints and effectively handling missing values. Due to these advantages, this study employs the Kalman filter.

The closed-loop control around the Kalman filter works as follows:

• The sender readies one or more collected samples to send every time slot of some length Δ^{RC}. The sender also has a threshold $\epsilon \in [0, 1]$ as a tolerance such that the prepared sample (individual or batch) will be transmitted only if the fractional difference between it and the previous value exceeds ϵ.

• The receiver predicts the values for the next time slot and continues to do so until it receives a transmitted sample from the sender. It then computes a measure of error η, which is accumulated for K time slots and then checked against the error threshold η_0. If $\eta > \eta_0$, the receiver estimates a new value of ϵ and sends it as feedback to the data sender.

• The purpose of the control mechanism is to make ϵ as large as possible (to reduce communications) and yet keep the signal reconstruction error at the hub within specified bounds. The mechanism thus provides an effective energy-accuracy tradeoff.

2.4 Control with Online Threshold Tuning

Alg. 1 shows the online threshold tuning performed by our controller on the signal receive side of the link. The algorithm gets the current threshold ϵ_{cur}, the actual value x_t, and the predicted value $\hat{x}_t$ and outputs the new threshold, ϵ_{new}. The algorithm uses the following parameters: (a) K, the gain of the controller, (b) Tol, the tolerance below which we would not replace the new with the old threshold, and (c) ϵ_{min} and ϵ_{max}, the lower and upper bounds for the threshold ϵ. In our application of the Kalman filter, a prediction will be made at every data collection instant (i.e., Δ^{RC} time apart).

Alg. 1: Online Threshold Tuning: Receive side
Input: $\epsilon_{cur}, x_t, \hat{x}_t$
Parameters: $K, Tol, \eta_0, \epsilon_{min}, \epsilon_{max}$
Output: ϵ_{new}
Initialize: $\eta_t \leftarrow x_t - \hat{x}_t$;
if ($|\eta_t| \le \eta_0$): $\epsilon_{new} \leftarrow \epsilon_{cur}$
else {
  $\epsilon_{new} \leftarrow \epsilon_{cur}(1 + K \cdot \eta_t)$
  $\epsilon_{new} \leftarrow \max(\epsilon_{min}, \min(\epsilon_{new}, \epsilon_{max}))$
  if ($|\epsilon_{new} - \epsilon_{cur}| < Tol$): $\epsilon_{new} \leftarrow \epsilon_{cur}$
}
Return: ϵ_{new}

Still, updates are made only when a new value arrives at the receiver. Online threshold adjustments are done by the hub at certain Δ_F frequencies, and the rate of Feedbacks/min is an important metric for this network. Suitable values for the gain K and Tol were determined experimentally, varying from sensor to sensor. In general, near-optimal values for such parameters can be obtained via a systematic search procedure.

2.5 Batch Transmission of Signals

Since CDMN sensors generate only a few bytes per sample, batching multiple samples before transmission reduces communication frequency with minimal overhead while allowing extended receiver sleep periods. This requires extending the Kalman filter to vector data, enabling Clustered Transmission (CT), which trades energy efficiency for latency—an acceptable compromise for fast signals. In CT, the sensor retains the previous data vector $v^{(prev)}$ as well. When the current vector $v^{(curr)}$ is complete, it computes the RMS value of the difference, i.e., $\sqrt{(\sum_{k=1}^{K}(v_k^{(curr)} - v_k^{(prev)})^2/K)}$ and compares it against the threshold to decide if $v^{(curr)}$ should be transmitted. In case of transmission, we let $v^{(prev)} = v^{(curr)}$. On the signal receive side, the Kalman filter predicts entire vectors, estimating error using the RMS difference between predicted and received vectors. This study evaluates Kalman filter performance as a function of batch size in CT.

3 Experimental Design and Results

We simulated a 5-node network with 2 hubs, one managing 3 nodes and the other 2 for energy-efficient communication using a Kalman filter-based approach. Energy consumption was quantified using

data sheet estimates, as detailed in [7]. Each sensor processed distinct data streams derived from publicly available physiological datasets.

3.1 Pre-processing of Datasets Used

All five sensors were simulated under varying monitoring durations ranging from 1 to 30 hours, with 1-hour increments. However, for clarity and consistency, results presented in this paper focus on a 1-hour monitoring period, as the behavior of the Kalman Filter applied in the sensors exhibited stable performance across longer durations.

Public datasets for continuous physiological monitoring are scarce, especially for implanted nodes. The dataset in [1] offers wearable-based BVP, IBI, and Blood Glucose data, which can be extended through subsampling and averaging for evaluation. Applied to four sensors, performance was assessed via Prediction Accuracy, Mean Absolute Error (MAE), Prediction Accuracy (100×(1−RMSE)), Rate of Native signals (Native Comms/min), Rate of Transmitted Signals(KF comms/min), and Number of Feedbacks Signals (Feedbacks/min).

Native Comms/min represents the transmission rate without closed-loop control (2 per minute, 120 per hour). KF Comms/min denotes the actual rate under closed-loop control, while Feedbacks/min quantifies threshold feedback signals from the hub to the sensors. All 120 hourly communications (2 per minute) would be transmitted without the proposed system. An offline-tuning approach was also evaluated using the mean of prior online tuning to explore the balance between communication reduction and prediction accuracy.

Physiological signals are typically stable but can change abruptly due to medical or emotional events, requiring rapid Kalman filter adaptation. To evaluate this, perturbations were introduced by doubling the signal magnitude at 15 minutes and halving it at 40 minutes. Sensors 1 and 2 processed BVP, while Sensors 3 and 4 handled IBI, with the latter exhibiting greater variability. Figs. 2(b), 3(b), 5(b), and 7(b) illustrate perturbations, marked by dashed lines (Doubled) and dotted lines (Halved).

3.2 Communications Accuracy vs. Frequency

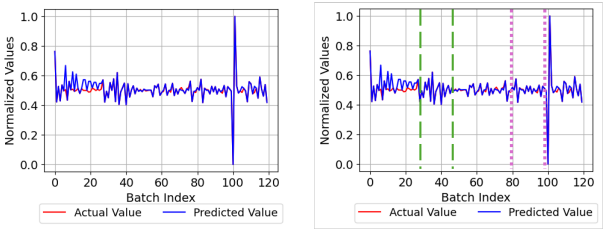

Fig. 2: Sensor 1 Prediction Performance (a) Without perturbation, (b) With perturbation

3.2.1 Sensor1 Communication. Table 3 highlights the stability of our controller under perturbations. As shown in Fig. 2(a) and Fig. 2(b), predicted (blue) and actual (red) values closely align, except during perturbations. While the unperturbed signal achieved 0.86% higher prediction accuracy, the perturbed case reduced KF Comms/min by 4.52%, balancing accuracy and efficiency. Despite a 9.12% MAE increase, our controller demonstrated rapid convergence, confirming its robustness to signal fluctuations within the intrabody network.

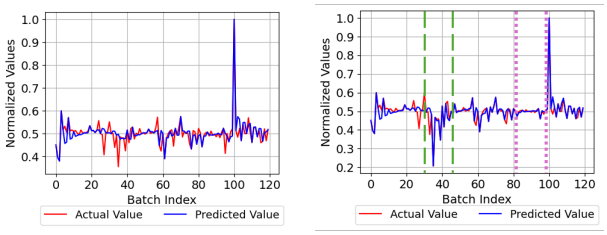

Fig. 3: Sensor 2 Prediction Performance (a) Without perturbation, (b) With perturbation

3.2.2 Sensor2 Communication. Fig. 3 compares actual and hub-predicted values for perturbed and unperturbed cases. The unperturbed signal (Fig. 3(a)) shows greater deviations between actual (red) and predicted (blue) values, whereas the perturbed signal (Fig. 3(b)) exhibits closer alignment. This improved coherence corresponds to a 58.46% increase in KF Comms/min due to higher Sensor 2 transmissions (Table 3).

The perturbed scenario increased MAE by 11.76% (Table 3) and reduced prediction accuracy by 0.68%. Fig. 4 illustrates the adaptive threshold adjustments by the controller, stabilizing at a lower level beyond batch index 38, in contrast to the larger fluctuations in the unperturbed signal before stabilizing around index 78. This indicates faster adaptation to increased signal variability.

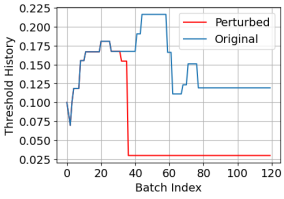

Fig. 4: Sensor 2 Threshold History w/ & w/o perturbations.

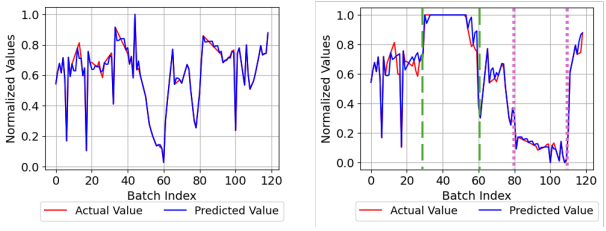

Fig. 5: Sensor 3 Prediction Performance (a) Without perturbation, (b) With perturbation

3.2.3 Sensor3 Communication. IBI signals exhibit greater sensitivity to perturbations, affecting prediction accuracy and communication efficiency. Fig. 5 compares actual and hub-predicted values. In the standard condition (Fig. 5(a)), significant fluctuations peak at batch index 39 (value 1) and drop to 0 at index 60, increasing KF Comms/min and Feedbacks/min (Table 3). In contrast, the perturbed condition (Fig. 5(b)) stabilizes at a peak from indices 30–54 and declines after index 81, reducing variability and KF Comms/min. Perturbations increased MAE by 9.68% and reduced prediction accuracy by 0.18%.

Fig. 6 further illustrates the online threshold adaptation. The perturbed signal shows higher initial threshold adjustments but stabilizes between indices 30–54, reducing Feedbacks/min. The unperturbed signal's threshold fluctuates before stabilizing at a lower level around index 45, whereas the perturbed signal stabilizes later (index 58) at a higher threshold, demonstrating the adaptability of closed-loop control.

3.2.4 Sensor4 Communication. Similar to Sensor 3, Sensor 4 exhibits significant variability under standard conditions, peaking at 0.9 (batch index 38) and dropping to 0.1 (indices 56, 58), increasing KF Comms/min and aligning actual (red) and predicted (blue) values in Fig. 7(a). Under perturbations (Fig. 7(b)), smoother variations led to stabilization at 1 (indices 30–52) and damping near 0.1 (indices 80–111), reducing KF Comms/min (Table 3).

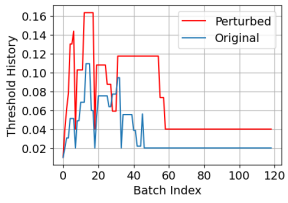

Fig. 6: Sensor 3 Threshold History w/ & w/o perturbations.

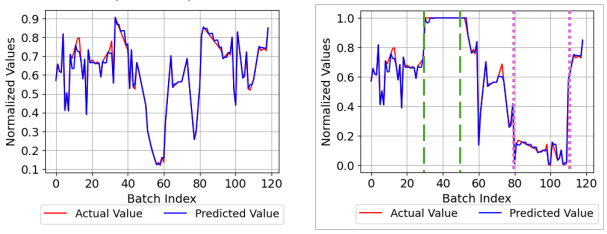

Fig. 7: Sensor 4 Prediction Performance (a) Without perturbation, (b) With perturbation

Table 3 further indicates a 1.67% drop in prediction accuracy, while improved communication efficiency highlights the trade-off between accuracy and energy conservation.

Fig. 8 shows that the threshold adjustments for the unperturbed and perturbed signals aligned until batch index 30, where the perturbed threshold increased with signal magnitude. The unperturbed signal stabilized at a lower level around index 43, while the perturbed signal required one more adjustment, stabilizing at a higher threshold near index 56. This adaptation reduced Feedbacks/min, demonstrating the response of our controller to signal perturbations.

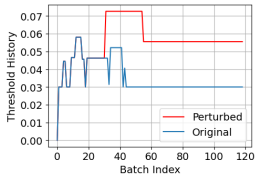

Fig. 8: Sensor 4 Threshold w/ & w/o perturbations.

3.3 Offline vs. Online Turning of Threshold

Table 2 compares our online threshold tuning approach against a simpler version where a suitable threshold is determined offline and then used without any further updates. The offline threshold reduced transmissions by 30.00% (vs. 25.83% for online) and eliminated hub-side feedback, which reduces communications; however, the online threshold adjustment yields slightly better accuracy.

For Sensor 2, both strategies performed identically, suggesting its data characteristics suit either approach. Sensor 3 exhibited minor accuracy loss and a slight MAE increase with the offline threshold, but communication efficiency remained unchanged.

Sensor 4 showed marginally higher communication savings with the offline strategy (40.00% vs. 39.17%) but slightly lower prediction accuracy, reinforcing the trade-off between accuracy and energy conservation.

Table 1: Sensor to Hub Transmission Performance

Signal	Performance Metric	Sensor Numbers 1	2	3	4
Unperturbed	MAE	0.060	0.034	0.093	0.074
	Pred. Acc. (%)	89.76	93.68	88.12	89.38
	Native Comms/min	2.0	2.0	2.0	2.0
	KF Comms/min	1.483	0.65	1.32	1.22
	Feedbacks/min	0.016	0.233	0.3	0.22
Perturbed	MAE	0.066	0.038	0.084	0.064
	Pred. Acc. (%)	88.99	93.04	87.31	87.89
	Native Comms/min	2.0	2.0	2.0	2.0
	KF Comms/min	1.416	1.03	1.0	0.967
	Feedbacks/min	0.016	0.167	0.166	0.167

Table 2: Impact of offline vs. online Threshold Tuning

Thres Type	Performance Metric	Sensor Numbers 1	2	3	4
online	MAE	0.0603	0.0344	0.0972	0.0741
	Pred. Acc.(%)	89.76	93.68	88.12	89.38
	Native Comms/min	2.0	2.0	2.0	2.0
	KF Comms/min	1.483	0.65	1.32	1.22
offline	MAE	0.0615	0.0378	0.0837	0.0754
	Pred. Acc.(%)	89.69	93.68	88.06	89.26
	Native Comms/min	2.0	2.0	2.0	2.0
	KF Comms/min	1.4	0.65	1.32	1.2
	Threshold Value	0.159	0.159	0.0285	0.0351

Table 2 shows that the offline threshold tuning conserves energy with minimal accuracy loss under stable conditions; however, online threshold tuning reduces prediction errors in high-variability data but increases communication. *The choice depends on whether energy efficiency or predictive accuracy is prioritized.*

3.4 Vector Data Transmission

A Clustered Time Series (CT) transmission approach was simulated to evaluate vector data behavior in intrabody networks, focusing on how vector size and error metrics affect transmission decisions and prediction accuracy. A vector $v^{(curr)}$ of size K is transmitted from the Hub Node 1 to the OBN when the Root Mean Square (RMS) error, defined as RMS Error $= \sqrt{\frac{1}{K}\sum_{k=1}^{K}\left(v_k^{(curr)} - v_k^{(prev)}\right)^2}$, exceeds a predefined threshold ϵ. Upon receiving the vector, the OBN employs a Vector Kalman Filter (VKF) to predict the next vector state, $v^{(predicted)}$. Prediction accuracy is measured using the equation $(100 \times (1-\text{RMSE}))$ and depicted in Fig. 9 against varying vector lengths.

To enhance communication efficiency and stabilize predictions, the closed-loop controller continuously adjusts the threshold ϵ based on the observed error between the predicted vector and the received vector and transmits feedback to the (physiological data sender) Node for adaptive control.

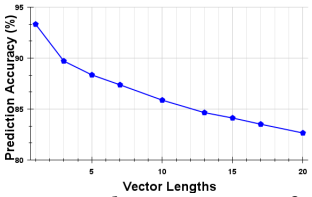

Fig. 9: Prediction Accuracy for Varying Vector Sizes

Fig. 9 shows that larger vector sizes slightly reduce prediction accuracy due to cumulative errors across dimensions. However, the VKF minimizes this loss by utilizing multidimensional correlations [10]. The decline results from element-wise prediction errors, delayed observation updates, and reduced sensitivity to temporal variations in larger vectors. These findings underscore the trade-off between communication efficiency and accuracy, highlighting the need to optimize vector sizes for energy-efficient physiological data transmission.

3.5 Simple vs. Adaptive Kalman Filter

Many versions of the Kalman Filter have been considered in the literature [5]. We use the standard version called the Simple Kalman Filter (SKF). Unlike the SKF, which assumes stationary noise with a fixed, offline-defined measurement noise covariance R, the adaptive Kalman Filter (AKF) variant adaptively adjusts R online using a sliding window of the 10 most recent measurements, thereby enhancing noise adaptability. Both filters were evaluated under unperturbed and perturbed conditions with identical state transition F, process noise covariance Q, and error covariance P for consistency.

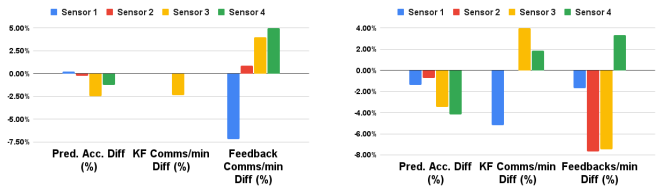

Fig. 10: SKF vs. AKF Performance Comparison (a) Unperturbed Signal, (b) Perturbed Signal

A comparison of Sensors 1–4 revealed minimal differences. For Sensor 1, the Adaptive Kalman Filter (AKF) slightly improved accuracy without affecting communication savings. Sensor 2 showed a slight decline in accuracy, but feedback signals were reduced while maintaining 67.50% communication savings. Sensor 3 exhibited lower accuracy, though feedback comms/min decreased significantly. Sensor 4 performed poorly in accuracy, and communication savings but showed reduced feedback comms/min. Perturbed signals exhibited similar behavior. Applying the AKF to perturbed signals does not produce any statistically significant performance improvements. On the contrary, the results indicate a deterioration in accuracy and effectiveness. These findings depicted in Fig. 10 indicate that AKF's added complexity provided negligible benefits over the Simple Kalman Filter (SKF). Given its lower computational cost and reliable performance, SKF was preferred for resource-constrained intrabody networks. Perturbation tests further confirmed its robustness with minimal impact on accuracy and communication metrics.

3.6 Performance Assessment of Noisy Signals

To emulate real-world acquisition imperfections, zero-mean Gaussian noise—scaled in the range of 5 - 10% of the signal's mean amplitude—was added element-wise to baseline BVP and IBI signals, yielding synthetic noisy data representative of practical sensing conditions. Simulations using the proposed controller revealed that the Simple Kalman Filter, in conjunction with optimized resampling, exhibited robust performance, achieving metrics comparable to those obtained under noise-free conditions. Experimental results demonstrate that the predictive accuracy of the system remains largely robust under Gaussian noise perturbations. For Sensor 1, a 5% noise amplitude resulted in an accuracy of 89.57%, with a marginal decline to 89.17% at 10%, both closely aligning with the noise-free accuracy of 89.76%. Sensor 2 exhibited negligible sensitivity to noise variations. In contrast, Sensor 3 experienced a minor accuracy reduction from 87.45% to 87.42% as noise amplitude increased. Similarly, Sensor 4 showed stable performance, with accuracy values of 88.66% and 88.31% for 5% and 10% noise levels, respectively. These results underscore the method's resilience to real-world noise contamination.

4 Conclusions

In this paper, we explored the trade-off between communication accuracy and energy efficiency via a closed-loop Kalman filter-based prediction of the signals. In most scenarios, communication overhead can be significantly minimized while preserving high accuracy. Given the substantial energy cost of transmissions, this approach effectively enhances energy efficiency. Future work will focus on continually tuning parameters for automatic adjustment, eliminating the need for manual intervention.

Table 3: Sensor to Hub Transmission Performance

Signal	Performance Metric	Sensor Numbers 1	2	3	4
Unperturbed	**MAE**	0.060	0.034	0.093	0.074
	Pred. Acc. (%)	89.76	93.68	88.12	89.38
	Native Comms/min	2.0	2.0	2.0	2.0
	KF Comms/min	1.483	0.650	1.320	1.220
	Feedbacks/min	0.016	0.233	0.300	0.220
	Comm. Reduction (%)	25.9	67.5	34.0	39.0
	Total Reduction (%)	25.1	55.9	19.0	28.0
Perturbed	**MAE**	0.066	0.038	0.084	0.064
	Pred. Acc. (%)	88.99	93.04	87.31	87.89
	Native Comms/min	2.0	2.0	2.0	2.0
	KF Comms/min	1.416	1.030	1.000	0.967
	Feedbacks/min	0.016	0.167	0.166	0.167
	Comm. Reduction (%)	29.2	48.5	50.0	51.7
	Total Reduction (%)	28.4	40.2	41.7	43.3

References

[1] Peter Cho, Juseong Kim, Brinnae Bent, and Jessilyn Dunn. 2023. Big ideas lab glycemic variability and wearable device data. *(version 1.1.1). PhysioNet.*

[2] Rajpreet Gulati, Krishna Kant, and Amitangshu Pal. 2022. Ultrasonic vs. magnetic resonance communication for mixed wearable and implanted devices. *Proc. of IEEE International Conf. on Communications (ICC)*, (May 2022), 5304–5309. DOI: 10.1109/ICC45855.2022.9838598.

[3] Sayemul Islam, Rajpreet Kaur Gulati, Michael Domic, Amitangshu Pal, Krishna Kant, and Albert Kim. 2022. Performance evaluation of magnetic resonance coupling method for intra-body network (ibnet). *IEEE Transactions on Biomedical Engineering*, 69, 6, (June 2022), 1901–1908. DOI: 10.1109/TBME.2021.3130408.

[4] Károly Kaszala and Kenneth A Ellenbogen. 2010. Device sensing: sensors and algorithms for pacemakers and implantable cardioverter defibrillators. *Circulation*, 122, 13, 1328–1340.

[5] Masoud Khodarahmi and Vafa Maihami. 2023. A review on kalman filter models. *Archives of Computational Methods in Engineering*, 30, 1, 727–747. DOI: 10.1007/s11831-022-09815-7.

[6] Hirsa Kia, Rajpreet Gulati, and Krishna Kant. 2024. A study of magnetic resonance and ultrasound based through-the-body communications. *Proc. of IEEE WiMob conference*, (Oct. 2024). DOI: 10.1109/WiMob61911.2024.10770313.

[7] Hirsa Kia, Pramita Pandit, and Krishna Kant. 2025. Energy transfer strategies in magnetic resonance based intrabody networks. *Proc. WoWMoM conf., Available at https://www.kkant.net/Hirsa_CDMN_energy_paper.pdf*, (Oct. 2025).

[8] World Health Organization. 2015. World report on aging. https://iris.who.int/bitstream/handle/10665/186463/9789240694811_eng.pdf. (2015).

[9] CR Powell. 2016. Conditional electrical stimulation in animal and human models for neurogenic bladder: working toward a neuroprosthesis. *Current bladder dysfunction reports*, 11, 4, 379–385.

[10] John Smith and Aditi Patel. 2022. Efficient communication in biomedical systems using kalman filters. *Journal of Biomedical Engineering*, 18, 4, 221–235. https://doi.org/10.1016/j.jbme.2022.221235.

[11] William J Tomlinson, Stella Banou, Christopher Yu, Milica Stojanovic, and Kaushik R Chowdhury. 2018. Comprehensive survey of galvanic coupling and alternative intra-body communication technologies. *IEEE Communications Surveys & Tutorials*, 21, 2, 1145–1164.

[12] D Werber, A Schwentner, and E M Biebl. 2006. Investigation of RF transmission properties of human tissues. *Advances in Radio Science*, 4, 4, (Sept. 2006), 357–360. DOI: 10.5194/ars-4-357-2006.